

ORIGINAL ARTICLE

Open Access



# Composite Behaviour of Textile Reinforced Reactive Powder Concrete Sandwich Façade Elements

Mathias Flansbjerg<sup>1</sup>, Natalie Williams Portal<sup>1\*</sup> , Daniel Vennetti<sup>1</sup> and Urs Mueller<sup>2</sup>

## Abstract

Within the EC funded project smart elements for sustainable building envelopes, carbon textile reinforcement was incorporated into reactive powder concrete, namely textile reinforced reactive powder concrete (TRRPC), to additionally improve the post-cracking behaviour of the cementitious matrix. This high-performance composite material was included as outer and inner façade panels in prefabricated and non-load bearing sandwich elements along with low density foamed concrete (FC) and glass fibre reinforced polymer continuous connecting devices. Experiments and finite element analysis (FEA) were applied to characterize the structural performance of the developed sandwich elements. The mechanical behaviour of the individual materials, components and large-scale elements were quantified. Four-point bending tests were performed on large-scale TRRPC-FC sandwich element beams to quantify the flexural capacity, level of composite action, resulting deformation, crack propagation and failure mechanisms. Optical measurements based on digital image correlation were taken simultaneously to enable a detailed analysis of the underlying composite action. The structural behaviour of the developed elements was found to be highly dependent on the stiffness and strength of the connectors to ensure composite action between the two TRRPC panels. As for the FEA, the applied modelling approach was found to accurately describe the stiffness of the sandwich elements at lower load levels, while describing the stiffness in a conservative manner after the occurrence of connector failure mechanisms.

**Keywords:** reactive powder concrete (RPC), textile reinforced concrete (TRC), foam concrete (FC), sandwich elements, four-point bending test, finite element analysis (FEA)

## 1 Background

Precast concrete façade elements for housing projects started to become a popular cladding solution at the end of the 1950s. Prefabricated modular concrete buildings were even constructed during the so-called *Million Program*, a public housing project realized in Sweden between the 1960s–1970s (Stenberg 2013). Similar residential housing projects were common in Europe during this era which supported the development of the concrete precast technique for the housing industry. Conventional steel reinforced concrete (RC) elements were dominating

the precast market for concrete building envelopes particularly during the 1960s–1980s. One of the main disadvantages of RC, however, is the inherent thickness of the concrete cover. Considering the exposure environment surrounding a building façade in Sweden, exposure classes of XC3/XC4 and a minimum cover thickness of 30–35 mm are recommended as per EN 206-1 (2013). This design requirement results in a total minimum thickness of an RC panel of approximately 80 mm, which, in turn, brings about particularly heavy and thick façade elements.

Over the past 15 years, new materials have emerged on the market enabling the thickness and weight reduction of precast concrete. Examples of such innovative materials include alternative reinforcements to conventional steel rebar, e.g. textile reinforcement, and

\*Correspondence: natalie.williamsportal@ri.se

<sup>1</sup> RISE Research Institutes of Sweden, Borås, Sweden

Full list of author information is available at the end of the article

Journal information: ISSN 1976-0485 / eISSN 2234-1315

high-performance concretes, e.g. ultra-high performance concrete (UHPC) or reactive powder concrete (RPC). Textile reinforced concrete (TRC) and UHPC have previously been used to produce façade elements in the form of ventilated façade cladding (Engberts 2006) or as sandwich elements (Hegger et al. 2008; Colombo et al. 2015; Shams et al. 2015). Progressively more UHPC/RPC has been used in façades, due to the fact that this type of high performance concrete demonstrates extraordinary high strength and durability (Miccoli et al. 2015; Ghoneim et al. 2010; Rebentrost et al. 2008). The addition of textile reinforcement to such a high performance matrix, designated here as textile reinforced reactive powder concrete (TRRPC), has been found to improve the post-cracking behaviour of high-strength concrete (Colombo et al. 2015; Mueller et al. 2016; Hegger et al. 2012).

The SESBE (smart elements for sustainable building envelopes) project, funded by the European Commission, focused on developing smart façade elements which are lighter, thinner and more adaptive than existing solutions through the utilization of nanomaterials and nanotechnology. The use of smart cost effective raw materials and cost saving technologies resulted in façade elements with increased energy efficiency, fire resistance and surface functionality. Prefabricated and non-load bearing sandwich façade elements were developed using a high-performance composite material, namely TRRPC, for the inner and outer layers, while low density foamed concrete (FC) made up the insulating core layer. Glass fibre reinforced polymer (GFRP) continuous connecting devices were incorporated to allow for partial composite action between the facing layers, all while minimizing the self-weight of the element and thermal bridges.

The aim of this paper is to present the evaluated structural performance of the TRRPC-FC sandwich façade elements developed within this project. The characterization of the structural performance of the developed sandwich elements was established through experiments and modelling. The experimental part of the program consisted of characterizing the mechanical behaviour for the individual materials, components and large-scale elements. Component tests were conducted to determine a suitable connector and panel design for the elements. Four-point bending tests were performed on large-scale TRRPC-FC sandwich element beams to quantify the flexural capacity, level of composite action, resulting deformation, crack propagation and failure mechanisms. Deformations were captured during flexural testing using an optical full-field deformation measurement system based on digital image correlation (DIC). Furthermore, numerical modelling based on finite element analysis (FEA) was applied to understand the connector

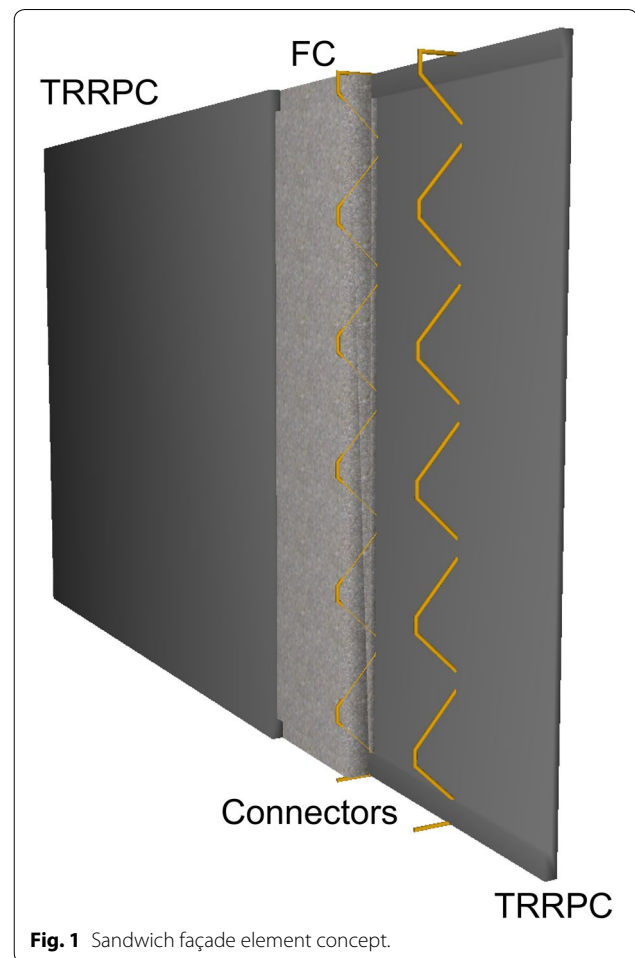


**Fig. 1** Sandwich façade element concept.

performance and the resulting composite action between the two RPC panels in the sandwich element.

## 2 Description of Façade Elements

### 2.1 Concept

The façade elements developed in this project are prefabricated concrete sandwich elements, which are intended to be attached to the main load-bearing structure by means of an anchorage system. Such elements are often categorized as architectural concrete cladding and have aesthetic, structural and isolating functions (fib 1998). The developed elements were designed to span vertically between two floor storeys and as such have a significant surface area (7–10 × 2.7–3.0 m) and weight (2–5 ton). Due to the element's large dimensions, these actively contribute in carrying and transferring loads, such as wind and self-weight, to the building. The façade elements are a combination of two TRRPC panels, whereby the outer and inner panels have a thickness of 25 mm. The TRRPC panels are separated by a 150 mm thick FC

insulating core material and attached with GFRP connecting devices, as illustrated in Fig. 1.

## 2.2 Applied Materials

### 2.2.1 Foam Concrete

FC is a lightweight cementitious material applied as a thermally insulating material. It principally consists of a combination of cement, sand, water and foam. According to project results, FC has around 70% lower embodied energy compared to expanded polystyrene (EPS) foam and possesses improved fire-safety properties such that it does not release smoke and toxic gases during a fire. In the project, FC was optimized with respect to density, compressive strength and heat conductivity. A wet density ranging between 200 and 300 kg/m<sup>3</sup> and a thermal conductivity in the range of 40–60 mW/(m K) were achieved. It was found that the thermal conductivity can be further decreased to 30–35 mW/(m K) with the addition of Quartzene® (Silva et al. 2015). Furthermore, short polypropylene fibres (12 mm), dosed at 0.25%-vol., were found to improve the post-cracking behaviour and handleability of the material. These additional materials were however not incorporated in the FC applied in the presented experiments.

### 2.2.2 Textile Reinforced Reactive Powder Concrete

TRRPC applied in this project consisted of an RPC reinforced by two layers of an epoxy coated carbon textile grid. An RPC formulation with higher amounts of supplementary cementitious materials (SCMs) was developed for use in prefabricated concrete façades. RPC is a variant of UHPC which has a maximum aggregate size of 2 mm or smaller. It is characterized as having a compressive strength above 120 MPa and a very low percentage of capillary pores. The RPC mix consists of six to eight different components; potentially rendering it sensitive to proportioning errors. A summary of the mechanical strength properties experimentally quantified for the developed RPC mix is provided in Table 1. Additional details pertaining to the development of the RPC mix can be found in (Mueller et al. 2016).

**Table 1 Summary of mechanical strength properties (28 days) for RPC, given as mean values and standard deviations in parenthesis. Source: (Mueller et al. 2016).**

Mix description	Compressive strength (MPa)	E-modulus (GPa)	Ultimate strain (‰)	Poisson's ratio (-)	Tensile strength (MPa)
RPC	147.2 (2.3)	49.7 (1.7)	3.89 (0.16)	0.216 (0.021)	5.14 (0.48)

The selected textile grid is an epoxy impregnated carbon textile grid (Solidian GRID Q85/85-CCE-21). The use of epoxy coating helps achieve superior bonding with the cementitious matrix. Through tensile tests of individual rovings, explained in Williams Portal et al. (2015) and illustrated in Fig. 2, the tensile strength and Young's modulus of the carbon textile grid in the longitudinal direction were 3433 MPa and 233 GPa, while those corresponding to transversal direction were 3878 MPa and 248 GPa, respectively. The measured strengths fall within the range specified by the producer.

### 2.2.3 Glass Fibre Reinforced Polymer Connectors

Truss-like connectors made of GFRP were incorporated in the sandwich element to enable sufficient composite action between the outer and inner RPC panels. The connectors were produced by Mostostal Warszawa S.A. within the scope of the project. The base material of the connectors consists of a pultruded bar of E-glass fibres impregnated with an epoxy resin having a nominal diameter of approximately 6.1 mm. The bars were wound with an additional bundle of fibres to form helical ribs on the surface, as shown in Fig. 3 (left). Moreover, the bars were formed into a zig-zag shape in a half-cured state and then cured into the final state in a subsequent step. Two connector configurations were investigated, namely single (S) and double (D), as illustrated in Fig. 3 (right). A double connector essentially consists of two single connectors which are mirrored with respect to the longitudinal direction and

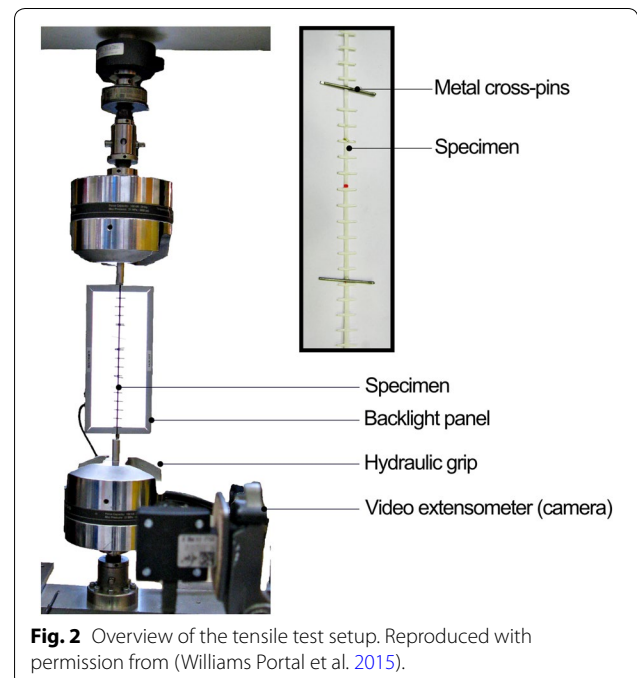


**Fig. 2** Overview of the tensile test setup. Reproduced with permission from (Williams Portal et al. 2015).

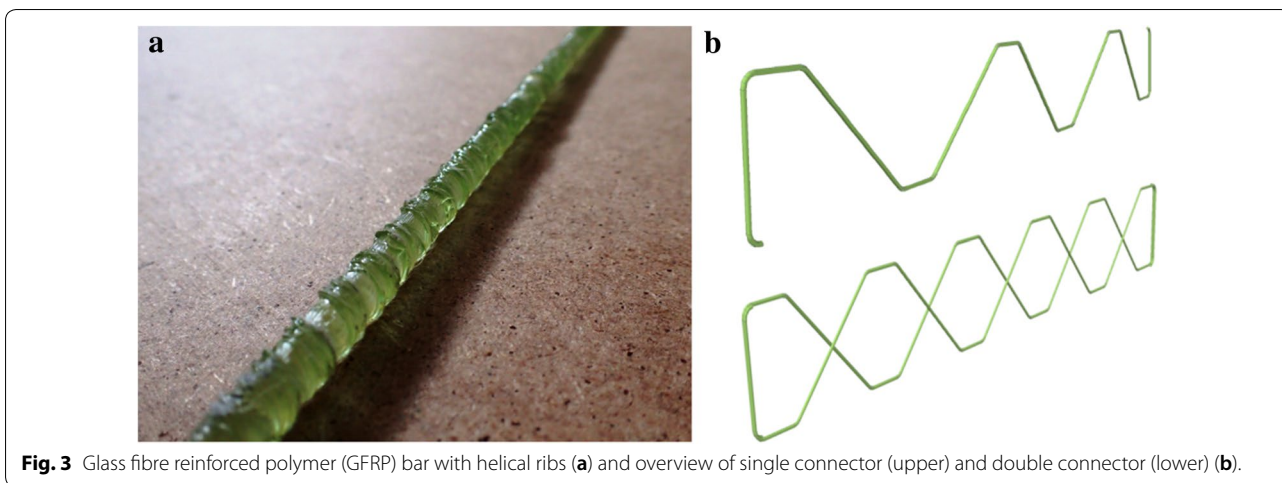


**Fig. 3** Glass fibre reinforced polymer (GFRP) bar with helical ribs (a) and overview of single connector (upper) and double connector (lower) (b).

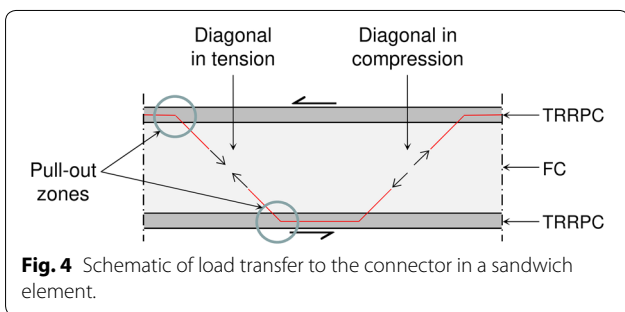


**Fig. 4** Schematic of load transfer to the connector in a sandwich element.

connected by plastic tie straps at intersecting points. When embedded in a sandwich element, the diagonal bars are mainly subjected to axial tensile and compressive forces, as depicted in Fig. 4.

### 3 Experimental Tests of Connectors

The connectors designed and applied in this project are intended to link the RPC panels in the sandwich element to ensure the adequate transfer of shear forces resulting in at least partial composite action. One of the underlying challenges of incorporating connectors in thin facings (25 mm) is being able to transfer force to the facings without achieving a local pull-out failure of the connector. Accordingly, an in depth experimental study was conducted within the framework of this project to evaluate the GFRP connectors on an individual material level as well as on a component level, i.e. incorporated in an RPC panel. The material level tests included tensile and compression tests, while pull-out and shear behaviour were tested on the component level. In the following, pertinent material and pull-out test results are presented. A detailed account of the component level testing can be found in (Flansbjerg et al. 2016).

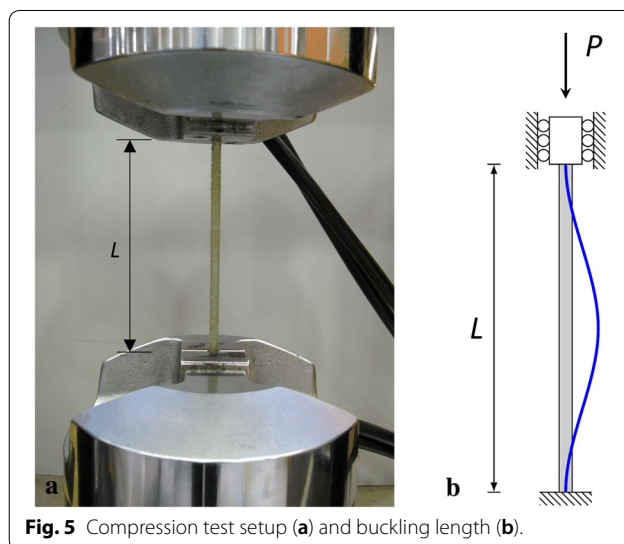


**Fig. 5** Compression test setup (a) and buckling length (b).

#### 3.1 Tensile Tests

Tensile strength tests of individual GFRP bar segments were performed according to ISO 10406-1 (2008), similar to that depicted in Fig. 2. Bars having a free length of 350 mm and a measurement length of 100 mm were tested. Steel tubes filled with epoxy resin ( $L = 100$  mm,  $\varnothing_{out} = 15$  mm and  $\varnothing_{in} = 12$  mm) were used as end anchorage for the bars. The tensile tests were conducted using a universal testing machine where the force was recorded using a 100 kN load cell. The tests were controlled by the cross-head displacement of 3 mm/min, corresponding to a strain rate of approximately 3%/min within the measuring length. The deformation of the bar was measured by a video extensometer based on a pattern recognition technique. The force and deformation were recorded with a sampling rate of 20 Hz. The experiments resulted in an average ultimate tensile

capacity of 29.9 kN, an average ultimate strain of 2.52% and an average Young's modulus of 40.3 GPa.

### 3.2 Compression Tests

Compression tests were performed on GFRP connector bar segments to determine the approximate buckling load using the same testing apparatus as for the tensile strength tests, as shown in Fig. 5a. The ends of the bar were placed in contact with the bottom of the grips and a clamp pressure of 1 MPa was applied. The load was applied with a displacement rate of 3 mm/min. Each grip had a clamp length of 65 mm, which allowed for a free buckling length between the grips while preventing the bar from rotating at the ends. This loading condition corresponds to Euler's fourth buckling case (refer to Fig. 5b).

The critical buckling load was determined experimentally for various buckling lengths of the GFRP bars (141–283 mm). The lengths were chosen to correspond to possible lengths of connector diagonals at an inclination of 45° to the TRRPC panel surface. The length is a function of the distance between the TRRPC panels which is controlled by the prescribed FC insulation thickness. The critical buckling load was observed to decrease with increasing buckling length; longer connector diagonals become less effective in compression. In a double connector, the compressed bars may become more effective due to a decreased buckling length, provided that the diagonals are attached at the intersections. For the selected thickness of 150 mm (samples with a free length of 212 mm), the average measured buckling load

was 1.72 kN. Based on the obtained results, a modulus of elasticity in compression was estimated to be 26.5 GPa. This value is significantly lower than that obtained in tension which is likely due to micro-buckling or kinking of the fibres within the matrix material (fib 2007).

### 3.3 Pull-out Tests

To be able to determine the relation between the embedment depth and pull-out strength of the GFRP connectors, small-scale pull-out tests were performed on connector segments embedded 10 mm in plain or textile reinforced RPC panels (50 × 400 × 400 mm), see Fig. 6a. A detailed account of a parametric study with differing embedment depths and connector types can be found in (Flansbjerg et al. 2016). The test specimen was positioned using an inclined supporting steel frame to introduce a load along the connector at an angle of 45° from the face of the RPC panel. Based on this loading condition, an axial force is introduced to the panel via the connector end, which is similar to the actual loading in the element (refer to Figs. 4 and 6b). The out of plane movement of the panel was prevented by two steel profiles, one on each side of the connector, whereby the free distance between the profiles was set to 200 mm. Thin fibre boards were placed between the steel profiles and the panel to avoid local stress concentrations. The in-plane movement of the panel was prevented by a steel profile along the upper panel edge.

The free ends of the GFRP bar connectors were manufactured with an anchoring system consisting of a steel

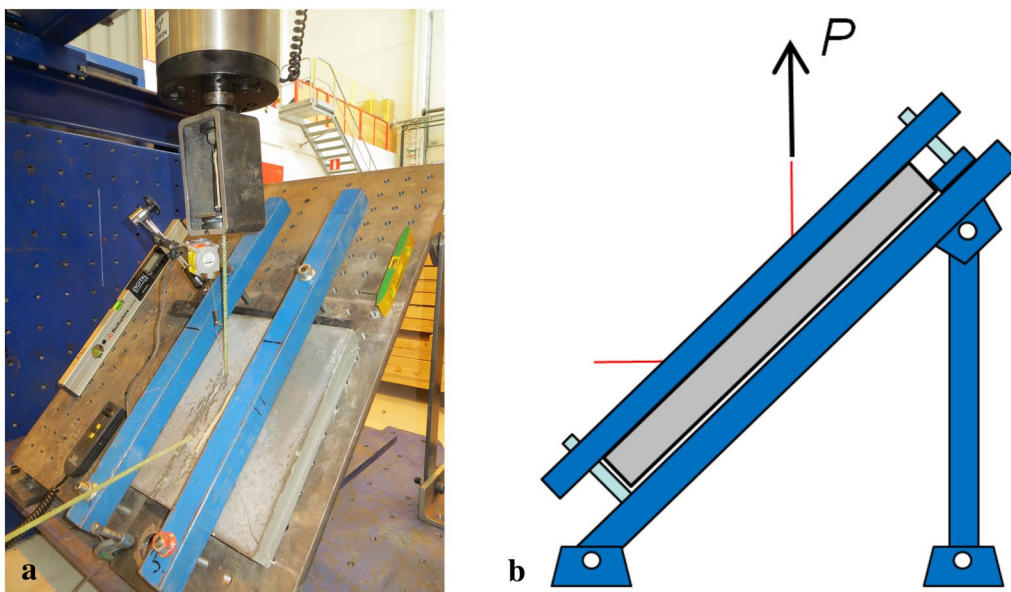


**Fig. 6** Pull-out test setup (a) and schematic of load transfer to connector (b).

tube filled with epoxy resin, which allows for the tensile force to be transmitted smoothly to the GFRP bars by shear stresses in the epoxy. A spherical bearing was placed between the end anchor and the loading device to ensure pure tensile force in the connector. The force was recorded using a load cell with a rated capacity of 100 kN and an accuracy better than 1%. The force and deformation were recorded in a data acquisition system with a sampling rate of 10 Hz. The load was controlled by a displacement rate of 1.0 mm/min. The pull-out capacity of the connectors was evaluated as the maximum force reached during testing. A brittle failure was generally observed due to spalling of the concrete cover. The specimens with carbon textile grid reached a higher average pull-out capacity of 6.5 kN compared to specimens with plain RPC having an average value of 4.1 kN.

### 4 Experimental Tests of Elements

#### 4.1 Test Description

Four-point bending tests were conducted on full-length beams of TRRPC-FC sandwich elements, as illustrated in Fig. 7, to primarily identify the connector performance and level of composite action. The results generated by these tests are also useful in determining the bending stiffness, cracking moment and bending moment resistance of the developed elements. Furthermore, the experimental outcome of the four-point bending tests is used in the validation of the numerical model presented in Sect. 5.

The test specimens consisted of two TRRPC panels with a nominal thickness of 25 mm and a FC insulation of 150 mm. The length and width of the specimen was set to 2.5 and 0.6 m. Both TRRPC panels were reinforced by two carbon textile grid layers connected to each other by distance spacers. The distance between the layers was 10 mm and the cover thickness of the outer layer was 5 mm. Two rows of connectors were placed longitudinally in each specimen at an edge distance of 100 mm, centre-to-centre spacing of 400 mm, and embedment depth of 10 mm. In this study, three specimens of both

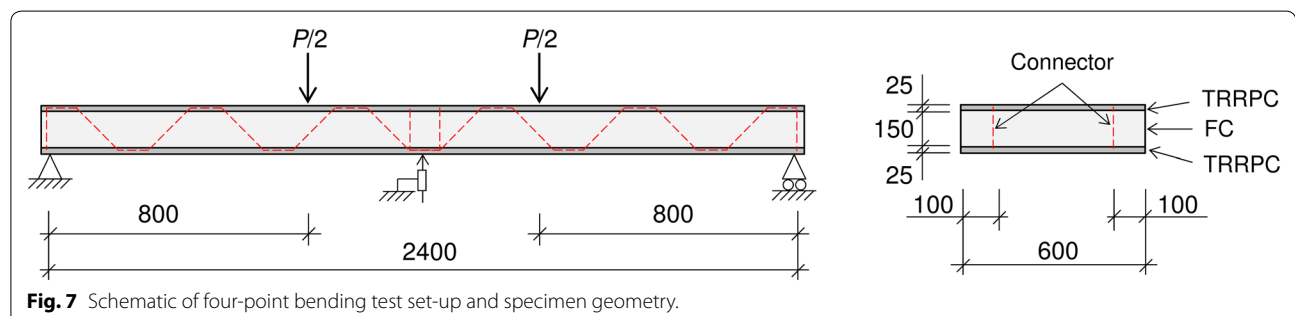
single and double configurations were tested, denoted as S-X (S-1 to S-3) and D-X (D-1 to D-3), respectively.

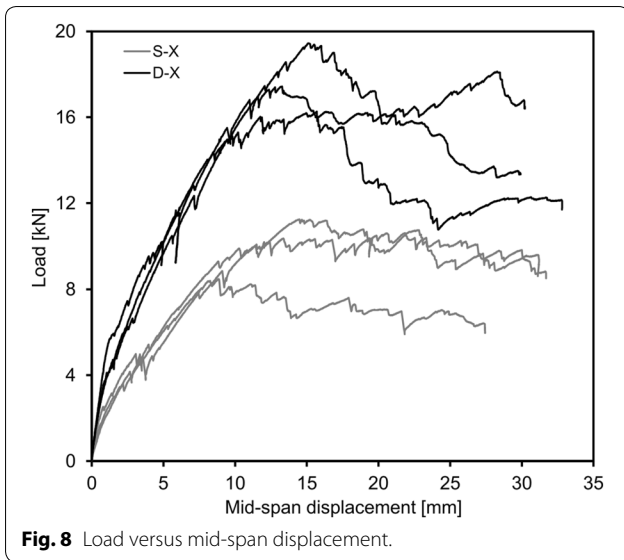
As depicted in Fig. 7, the specimens were placed on two end supports, with a centre distance,  $L$ , of 2.4 m. The specimens were loaded by two upper line loads each applying a load of  $P/2$ , which were 0.8 m apart. The tests were performed in a servo hydraulic testing machine and the load was applied quasi-statically in displacement control with a rate of 5 mm/min. During testing, the mid-span deflection of the element was measured using a linear variable displacement transducer (LVDT) with a measuring range of 100 mm and a relative error less than 1.5%. The rated capacity of the load cell was 100 kN with a relative error within 1%, while the displacement and the load were recorded at a rate of 20 Hz.

Optical deformation measurements were performed along one side of the element to capture the displacements of the two TRRPC panels. Measuring markers were attached to the upper and lower panels every 200 mm. The image acquisition was performed using the optical system ARAMIS 12 M and the evaluation was executed in GOM Correlate Professional V8 (GOM 2015). The system uses a measurement technique based on digital image correlation (DIC). The system was set up as two individual 2D measurements (measuring area  $1.4 \times 1.0 \text{ m}^2$ ), each camera covering half the beam, with a small overlap at the centre. For this configuration, the coordinate measurement accuracy was approximately  $3 \mu\text{m}$  and the image capture frequency was 1 Hz.

#### 4.2 Quantification of Composite Action

The bending behaviour of the two specimen configurations, in terms of load versus mid-span displacement from LVDT measurements, is compared in Fig. 8. The initial stiffness of the composite element is less for the single connector configuration compared to the double connector configuration. First cracking also occurs at a slightly lower load level,  $P_{cr}$ , for the S-X specimens, which is followed by a loss of stiffness. Upon reaching the maximum load,  $P_{max}$ , the S-X specimens undergo a





significant loss of stiffness depicted by a nearly horizontal plateau which is believed to signify the event of connector pull-out. In relation to the specimens with double connectors, the specimens with single connectors, S-X are shown to exhibit approximately 40% of the experimental bending stiffness in the uncracked stage and 57% of the load resistance. An interesting observation to note is that all samples displayed a relatively ductile failure even though both RPC and GFRP are considered to be brittle materials.

The load at the first bending crack determined from load–displacement curves, and the first peak load obtained during testing are summarized in Table 2. Also tabulated are the corresponding crack moment,  $M_{cr}$ , and first peak bending moment,  $M_{max}$ , which are calculated from the static equilibrium condition of the four-point bending set-up as per Eq. 1 (refer to Fig. 7).

$$M = \frac{Pa}{2} \tag{1}$$

The structural behaviour of the sandwich elements depends highly on the stiffness and strength of the GFRP connectors to ensure composite action, i.e. provide longitudinal shear transfer between the inner and outer TRRPC panels. Sandwich elements can be categorized according to different degrees of composite action, as illustrated in Fig. 9: (a) fully composite, (b) partially composite or (c) non-composite element. The fully composite action signifies that all parts of the element act together to resist the bending moment as a unit, reflected in strain distribution remaining essentially linear across the section (Fig. 9a). Concerning full composite action, the element fails either by concrete crushing or tensile rupture of the carbon textile grid before failure of the connectors occurs. For this failure mode to ensue, connectors with very high stiffness and strength are needed which is often difficult to achieve in reality. If the panels are connected by means of connectors without longitudinal shear transfer capacity, e.g. straight pin connectors, the element can be considered as non-composite. In such a case, the panels are forced to have the same curvature and act more or less independently with a strain distribution across the section according to Fig. 9c. When the connectors can only transfer a portion of the shear forces required for fully composite action, the element can be considered as partially composite with a strain variation across the

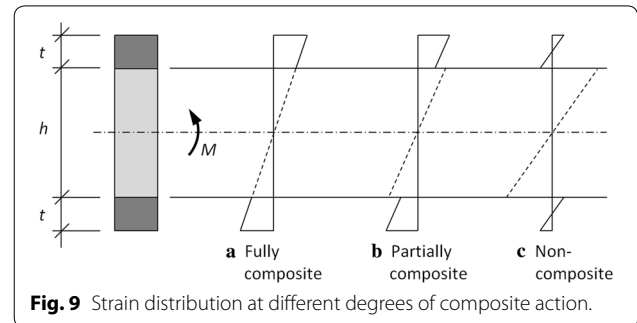


**Table 2** Summary of four-point bending results for single and double connector configurations.

Specimen ID	Crack load $P_{cr}$ (kN)	Crack moment $M_{cr}$ (kNm)	Max load $P_{max}$ (kN)	Max moment $M_{max}$ (kNm)	Bending stiffness $EI_{test}$ (kNm <sup>2</sup> )	Composite action $\alpha$ (–)	$EI_1/EI_{test}$ (%)	$\alpha EI_2/EI_{test}$ (%)
S-1	3.8	1.5	8.5	3.4	415	0.021	33	67
S-2	3.2	1.3	11.3	4.5	510	0.029	26	74
S-3	4.2	1.7	10.6	4.2	399	0.020	34	66
Avg (std)	3.7 (0.4)	1.5 (0.2)	10.1 (1.2)	4.0 (0.5)	441 (49)	0.023 (0.004)	31 (3)	69 (3)
D-1	5.7	2.3	19.4	7.8	1247	0.085	11	89
D-2	3.7	1.5	17.4	7.0	1038	0.069	13	87
D-3	4.3	1.7	16.3	6.5	935	0.061	14	86
Avg (std)	4.6 (0.8)	1.8 (0.3)	17.7 (1.3)	7.1 (0.5)	1073 (130)	0.071 (0.010)	13 (1)	87 (1)

section as per Fig. 9b. For the partially composite scenario, the connectors fail before concrete crushing or the rupture of carbon textile grid.

The bending stiffness,  $EI$ , of the uncracked sandwich beam section, in the case of full composite action, is the sum of the bending stiffness of the RPC panels and the FC insulation with respect to the centroid axis of the entire section, expressed as Eq. 2:

$$EI = E_{RPC} \frac{bt^3}{6} + E_{RPC} \frac{bt(h+t)^2}{2} + E_{FC} \frac{bh^3}{12} \quad (2)$$

$$= EI_1 + EI_2 + EI_3$$

where  $E_{RPC}$  and  $E_{FC}$  are the moduli of elasticity of RPC and FC, respectively;  $t$  is the thickness of the panels;  $h$  is the thickness of the insulation layer; and  $b$  is the width of the beam.

The first term,  $EI_1$ , is the bending stiffness of the two individual RPC panels about their own neutral axis. The second term,  $EI_2$ , is the bending stiffness of the panels associated with bending about the neutral axis of the entire element, which is derived according to the parallel axis theorem. Finally, the third term,  $EI_3$ , is the bending stiffness of the FC insulation. Since the stiffness of FC is much lower than that of RPC ( $E_{FC} \ll E_{RPC}$ ), the third term is assumed to be insignificant and is neglected. To distinguish between the two remaining terms,  $EI_1$ , is the bending stiffness in the case of non-composite action where the two panels act independently (Fig. 9c), while  $EI_2$  is the additional contribution as a result of full composite action. Consequently, the bending stiffness related to partially composite action must lie between these two extremes. The bending stiffness can be expressed for different degrees of composite action by introducing a composite action factor  $0 \leq \alpha \leq 1$ , where  $\alpha = 0$  signifies non-composite action and  $\alpha = 1$  implies full composite action (see Eq. 3).

$$EI = E_{RPC} \frac{bt^3}{6} + \alpha E_{RPC} \frac{bt(h+t)^2}{2} = EI_1 + \alpha EI_2 \quad (3)$$

Furthermore, the elastic deflection,  $\delta$ , at the mid-span of a beam in four-point bending with point loads ( $P/2$ ) placed at the third points ( $a=L/3$ ) of the span,  $L$ , as illustrated in Fig. 7 can be calculated as:

$$\delta = \frac{Pa(3L^2 - 4a^2)}{48EI} = \frac{23PL^3}{1296EI} \quad (4)$$

From Eq. 4, the bending stiffness can be calculated as:

$$EI = \frac{23PL^3}{1296\delta} \quad (5)$$

The bending stiffness of the tested beams can therefore be evaluated from the load–deflection curves by evaluating the secant modulus between two points ( $P_1, \delta_1$ ) and ( $P_2, \delta_2$ ) in the uncracked stage as:

$$EI_{test} = \frac{23L^3}{1296} \cdot \left( \frac{P_2 - P_1}{\delta_2 - \delta_1} \right) \quad (6)$$

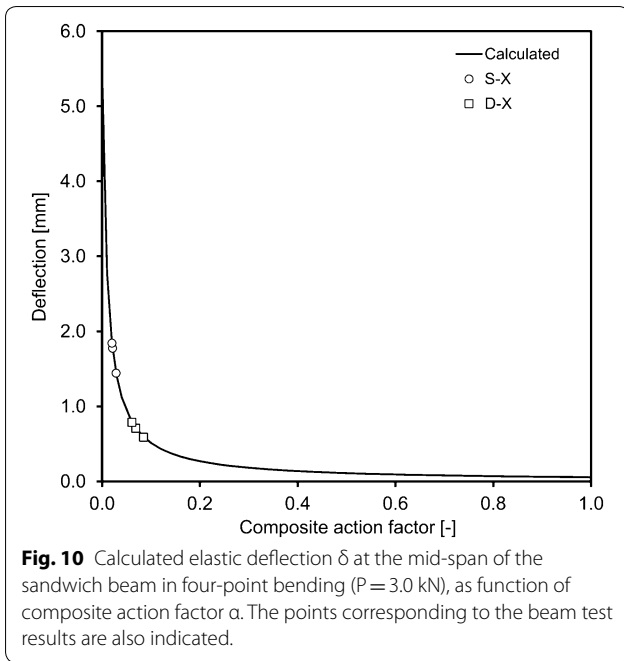
The load levels in the uncracked stage were generally chosen as  $P_1=0.5$  kN and  $P_2=3.0$  kN. Given that the experimental bending stiffness is known, the composite action factor,  $\alpha$ , of the beam can be determined by setting  $EI = EI_{test}$  in Eq. 3, accordingly:

$$\alpha = \frac{EI_{test} - EI_1}{EI_2} \quad (7)$$

The modulus of elasticity for RPC is  $E_C=50$  GPa derived from material tests earlier reported in Sect. 2.2. As per Eq. 2, the two terms of the calculated bending stiffness amount to  $EI_1=135$  kNm<sup>2</sup> and  $EI_2=13.0$  MNm<sup>2</sup>. The determined bending stiffness and the composite action factors are presented in Table 2 for all tested specimens.

The double connector configuration provides significantly higher bending stiffness compared to the single connector configuration. It was observed that the composite action factor  $\alpha$  was calculated to be rather low in both cases; in average 0.023 for the S-X beam specimens and 0.071 for the D-X specimens. Since the bending stiffness increases linearly with the composite action factor and the deflection is denoted by the inverse of the bending stiffness, the deflection decreases with the inverse of the composite action factor. According to this relation, even a low composite action factor has a significant effect in reducing the deflection, as per Fig. 10. From Table 2, the second term of the bending stiffness ( $\alpha EI_2$ ), representing the effect of composite action, in average stands for 69 and 87% of the total bending stiffness for the beam specimens with single connectors (S-X) and with double connectors (D-X), respectively. In the extreme case where a non-composite behaviour is governing, the thickness of each TRRPC panel needs to be increased to 45 mm (S-X case) and 60 mm (D-X case) to achieve the bending stiffness yielded in the experiments.

From Fig. 10, it is insignificant to strive for very high composite action, as the effect in reducing the deflection declines significantly with an increasing composite action factor. Since the composite action is directly related to the connector configuration, it is important to remember that the presented values of bending stiffness and composite action factor are only valid for a sandwich element with a connector spacing of approximately 300 mm.



Consequently, an increase in connector spacing reduces the composite action factor and in turn the bending stiffness.

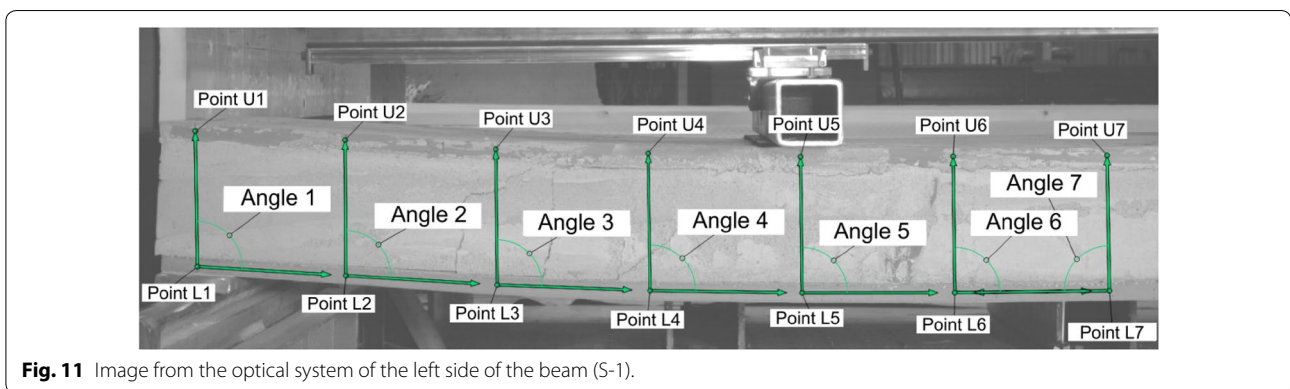
### 4.3 Optical Measurements

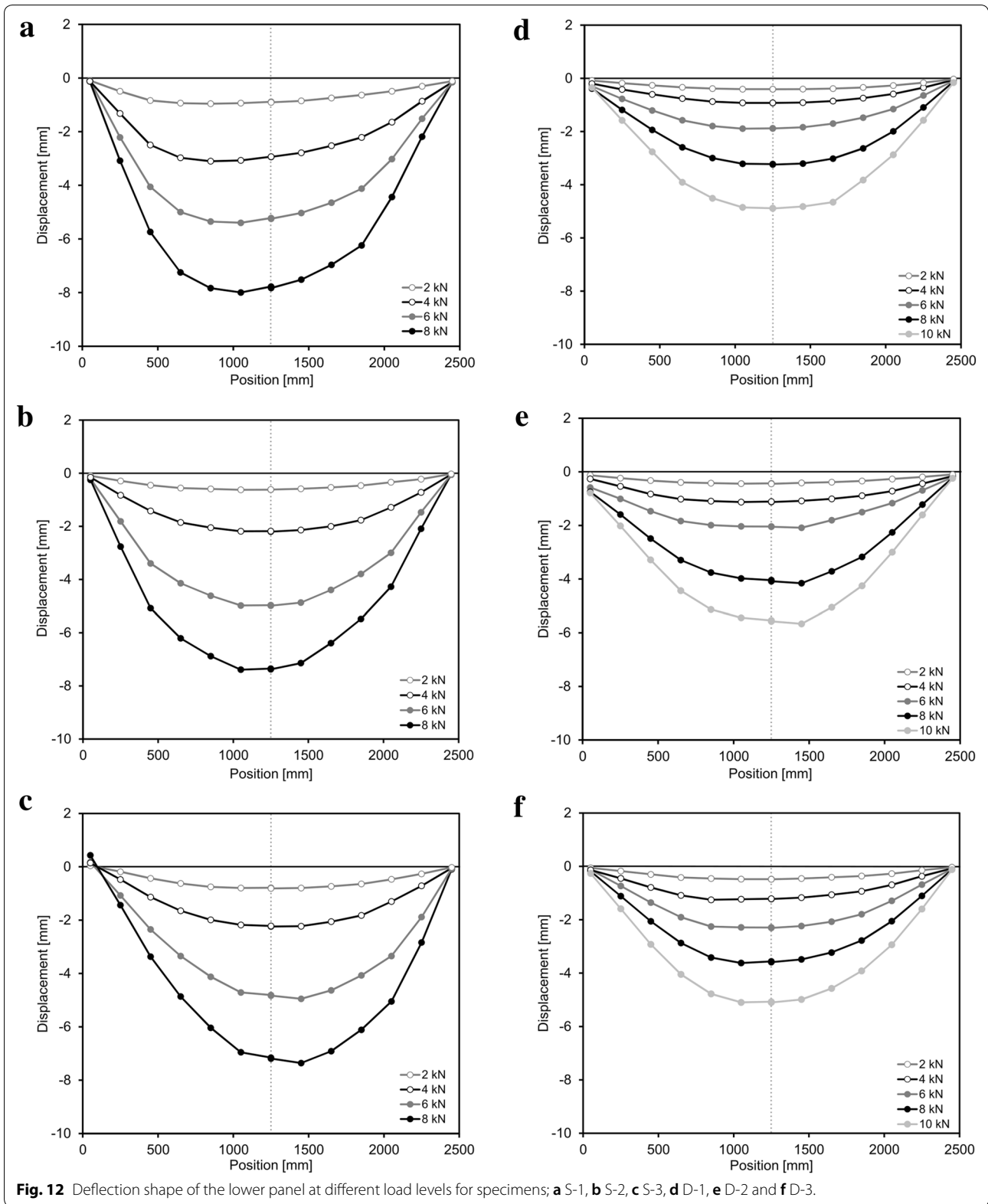
Optical measurements enabled a more detailed analysis of the flexural behaviour in relation to the deflection shape and relative displacement between the panels. Measuring points were defined on the upper and lower TRRPC panels to capture the localized displacement at each of these points during testing, as indicated in Fig. 11. The deflection shape of the lower panel was evaluated at different load levels for both connector configurations, as depicted in Fig. 12. Specimens with D-X exhibit smaller deformations and a more

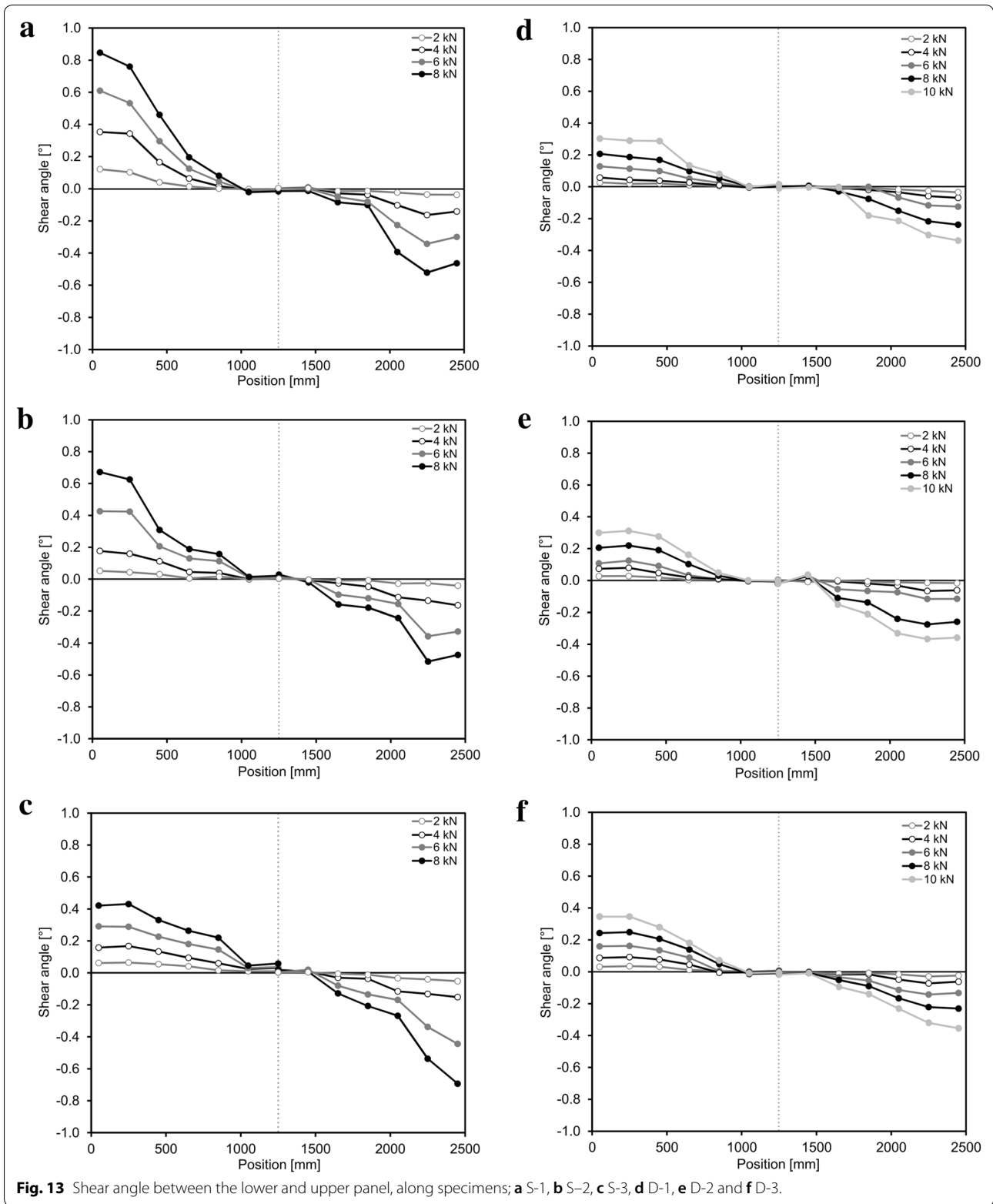
symmetric deflection shape compared to the specimens with S-X. For instance, at a load level of 4 kN, which is within the region of  $P_{cr}$  for S-X, the average maximum displacement noted for S-X is 2.5 mm which is slightly more than double that observed for D-X (1.1 mm). When approaching  $P_{max}$  for S-X (8 kN), the average maximum displacement for S-X (7.6 mm) is still approximately double that yielded for D-X (3.7 mm).

The amount of relative longitudinal displacement between the two panels is a result of the degree of composite action. The relative displacement can also be represented as the shear angle between the panels as measured in the optical system. A shear angle is calculated at 13 locations along the beam, as indicated in Fig. 11, which corresponds to the change in angle defined by three reference points, namely  $U_N$ ,  $L_N$  and  $L_{N+1}$ , where the index  $N$  refers to the reference point number. In the case of full composite action, there is no relative displacement between the panels, which corresponds to a shear angle of zero. For a simply supported beam, the relative displacement is zero at mid-span and maximum at the supports. The displacement increases as the degree of composite action decreases. The shear angle is approximately zero at the middle of the specimen and increases in absolute values towards the ends, as shown in Fig. 13. Here, the D-X configuration provides more composite action, as the shear angle is smaller, compared to the specimens with S-X at the same load level. From the images recorded during the optical measurements, it was observed that a relative slip occurred at the interface between the FC and the lower RPC panel during testing in all cases. This observation is thought to be an effect of the layer casting procedure, which involved the casting of the FC core on top of the lower RPC panel, followed by the casting of the upper RPC panel on top of the FC.

The development of the shear angles at the ends of the beams, i.e. 50 and 2400 mm, are plotted against the







normalized load, being the ratio between the load and the maximum load for each specimen ( $P/P_{max}$ ), in Fig. 14. A general observation is that the shear angle gradually increased at the beam ends due to increased loading. The shear angle increased between 30 and 40% of  $P_{max}$  which is thought to correspond to first cracking. After this point, the load continued to increase until reaching the maximum load marked by a ratio of 1.0. Subsequently, the load either remained relatively constant or decreased followed by further development of the shear angle at one end of the beam. This observed behaviour is thought to be a consequence of a connector failure occurring around maximum load, thus leading to lower longitudinal shear stiffness and increased relative displacements between the panels.

**4.4 Post-test Observations**

To understand the underlying failure mechanisms occurring during bending testing, the FC was removed from the core of the sandwich elements to enable the visual inspection of the connectors and inner surfaces of the concrete panels. It was identified that the failure of all specimens was related to local spalling of the TRRPC cover at most of the connector points on the side of the beam which experienced a noticeable increase in shear angle after achieving maximum load (see Fig. 14). Moreover, several connector bars subjected to compression were found to have buckled. In some cases, concrete spalling was apparent in the vicinity of connectors located on the side of the specimen experiencing smaller shear angles. Typical observations of cover spalling and connector failure are depicted in Fig. 15.

The localized embedment depths of the pulled-out connectors were measured to be 6–11 mm which marginally deviates from the nominal depth of 10 mm. This measured deviation in embedment length is caused by production and human error. In view of that, a correlation can be noted between the elements having smaller connector embedment depths and resulting lower load capacity previously listed in Table 2 (results from Sect. 4.2).

**5 Modelling of Composite Action**

**5.1 Modelling Parameters**

To gain better insight into the composite action of the sandwich elements, finite element (FE) calculations of the four-point bending tests (refer to Sect. 4) were performed using Abaqus/CAE 6.14-1 (2014). The model encompasses the discrete parts for the TRRPC panels, FC,

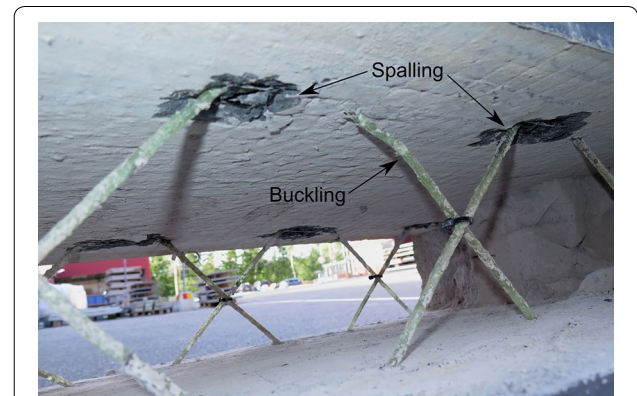


**Fig. 15** Example of typical cover spalling at connector bars in tension and buckling of compressed connector bar.

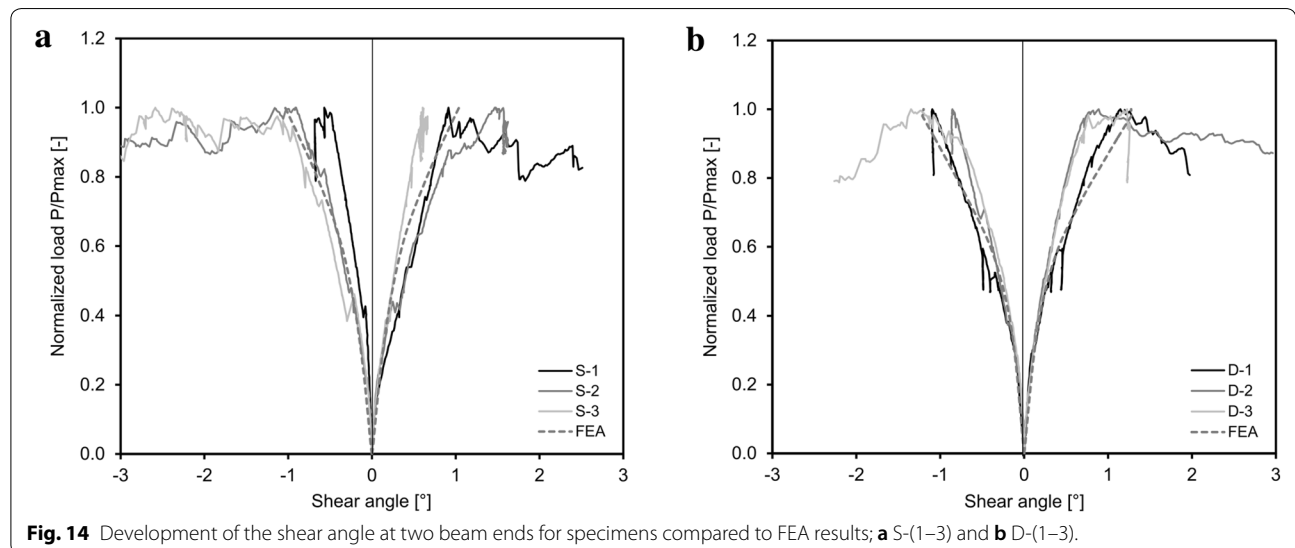


**Fig. 14** Development of the shear angle at two beam ends for specimens compared to FEA results; **a** S-(1–3) and **b** D-(1–3).

GFRP connectors and loading devices, as illustrated in Fig. 16. The loading equipment was modelled using rigid body constraints. The upper panel was attached to the FC using tie constraints which assumes that a full interaction exists at the interface. The interface between the lower panel and the FC was modelled using a frictionless contact condition, which was defined based on observations of relative slip occurring at this interface during four-point bending and shear tests reported elsewhere (Flansbjerg et al. 2016). It is thought that this phenomenon is likely an effect of the layer casting procedure, consisting of the FC being cast on top of the lower TRRPC panel followed by the upper TRRPC panel being cast on top of the FC. In the model, the connectors were attached to the centre of the panel thickness using tie constraints to allow for actual connector geometries. Furthermore, the analysis consisted of initially subjecting the beam to the self-weight of the different components followed by applying load through a forced displacement of the loading equipment.

The TRRPC panels and FC insulation were modelled using 8-node linear continuum shell elements (Dassault Systèmes Abaqus/CAE User's Guide 2014). Shell elements are typically used to model structures in which one dimension, namely the thickness, is significantly smaller than the other dimensions. From a modelling point of view, continuum shell elements are comparable to three-dimensional continuum solids, but their kinematic and constitutive behaviours are more similar to conventional shell elements. These elements are specified according to full three-dimensional geometry and the element thickness is defined by nodal geometry. Only displacement degrees of freedom at the nodal points are associated with these elements.

The FC was assumed to have a density of  $300 \text{ kg/m}^3$  and a linear elastic material behaviour with assumed values for the modulus of elasticity (10 MPa) and Poisson's ratio (0.1). The behaviour of the RPC was taken into account

using a continuum, plasticity-based, damage model for concrete (Dassault Systèmes Abaqus/CAE User's Guide 2014). It assumes that the two main failure mechanisms are tensile cracking and compressive crushing of the concrete material. As the compressive stresses in the panels were estimated to be low, a linear elastic model was used to describe the RPC behaviour in compression. Under uniaxial tension, the stress–strain response follows a linear elastic relationship until the value of the failure stress is reached. The failure stress corresponds to the onset of micro-cracking in the concrete material. Beyond the failure stress, the formation of micro-cracks is represented macroscopically with a softening stress–strain response, which induces strain localization in the concrete structure. The tensile strength of RPC was set to 3.0 MPa, which corresponds to the measured tensile strength of RPC reinforced by two layers of carbon textile grid. The results pertaining to these uniaxial tensile tests are published elsewhere (Mueller et al. 2017). Moreover, a linear softening behaviour was defined with a fracture energy value of  $70 \text{ Nm/m}^2$ . The modulus of elasticity in both tension and compression (50 GPa) as well as Poisson's ratio (0.22) were described using experimental data obtained from material tests presented in Sect. 2.2.

The carbon textile grid is included in the FE model as embedded reinforcement layers in the shell elements, which assumes a perfect bond between the reinforcement and the concrete. Linear elastic material models were used to describe the behaviour up to failure of the reinforcement. Experimentally data (refer to Sect. 2.2) were included for the modulus of elasticity (233 GPa) and nominal tensile strength of the bars (3433 MPa). For simplicity, the same properties were used in both the longitudinal and transversal directions of the grids.

The GFRP connectors were modelled using linear beam elements (Dassault Systèmes Abaqus/CAE User's Guide 2014). The beam elements were attached to the centre of the continuum shell elements, representing the panels, using tie constraints. At the connector-FC interface, no interaction was defined such that the connectors were assumed free to buckle. A linear elastic material behaviour was used to describe the GFRP bars. Experimentally quantified values (refer to Sect. 3) were included for the modulus of elasticity (40.3 GPa) and nominal tensile strength of the bars (1012 MPa), while a Poisson's ratio of 0.3 was assumed. With this formulation, the possibility of buckling of the GFRP bars is accounted for in the model but the limitation of the GFRP bars due to pull-out must be considered as a post processing step. An initial connector imperfection of 0.5 mm was taken into account in the model. Both single and double connector configurations were modelled using the same procedure.

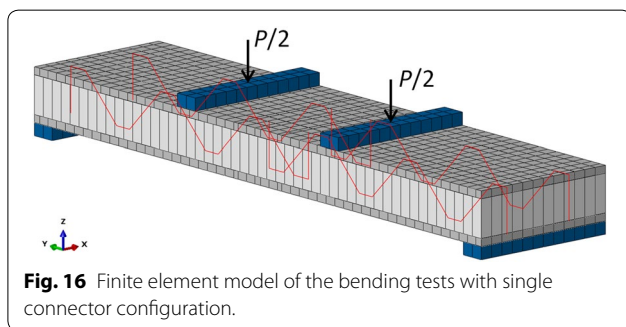


**Fig. 16** Finite element model of the bending tests with single connector configuration.

## 5.2 Validation with Experimental Results

The modelling approach is validated using the four-point bending experimental results presented in Sect. 4. The presented validation particularly focuses on analysing the resulting performance of the connectors, composite action and crack formation.

### 5.2.1 Connector Performance

A comparison of the load versus mid-span deflection curves from the beam tests and FE analyses is shown in Fig. 17 for both connector configurations. Load levels at which the most stressed connectors start to buckle and reach the average pull-out capacity are also indicated. For both configurations, the stiffness at lower load levels ( $\leq 5$  kN) correlates rather well with that of the experimental results, however the computed stiffness becomes lower than the experimental stiffness as the load increases. The stiffness of the sandwich element appears to be largely governed by the stiffness of the connectors, which, in turn, partly depends on the buckling of the compressed bars in the connectors. At the applied loads indicated in Fig. 17, 3.9 kN (S-FE) and 7.1 kN (D-FE), the maximum compressive force in the modelled GFRP bars corresponds to the experimental buckling load (1.72 kN) presented in Sect. 3.2. The observed differences in stiffness between the experimental and computed results are thought to be primarily since the connectors were assumed free to buckle in the model whereas the FC, in reality, provides some resistance to buckling. A conservative model has been applied as the true interaction between FC and the connectors involves many uncertain parameters which have not been measured in this study.

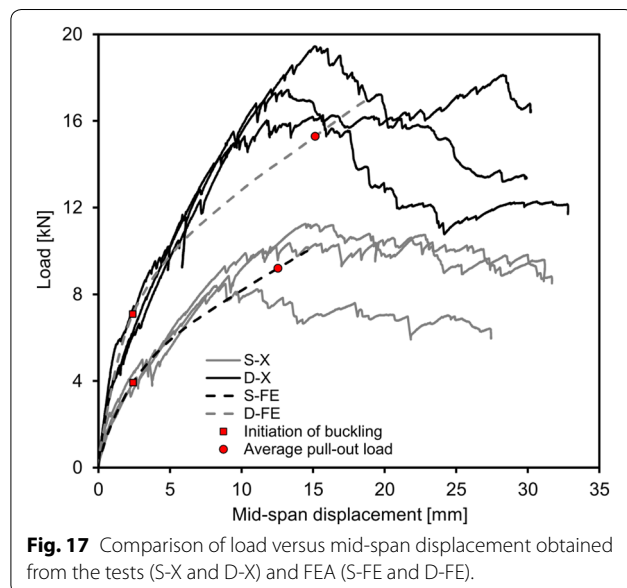


**Fig. 17** Comparison of load versus mid-span displacement obtained from the tests (S-X and D-X) and FEA (S-FE and D-FE).

From the four-point bending tests, it was observed that the failure process was governed by the connector capacity, or more specifically the initiation and progression of connector pull-out from the TRRPC panels. Since a description of the pull-out failure process is not included in the FE-model, this phenomenon is not explicitly captured. Nevertheless, the forces in the connector from the analysis can be compared to the experimental pull-out capacity of a single connector (6.5 kN) mentioned in Sect. 3.3. From Fig. 17, the applied load levels, 9.2 kN (S-FE) and 15.3 kN (D-FE), in which the modelled GFRP bars have a maximum tensile force equal to the tested pull-out load, correspond rather well with the level at which the pull-out failure process starts in the tests for both connector configurations.

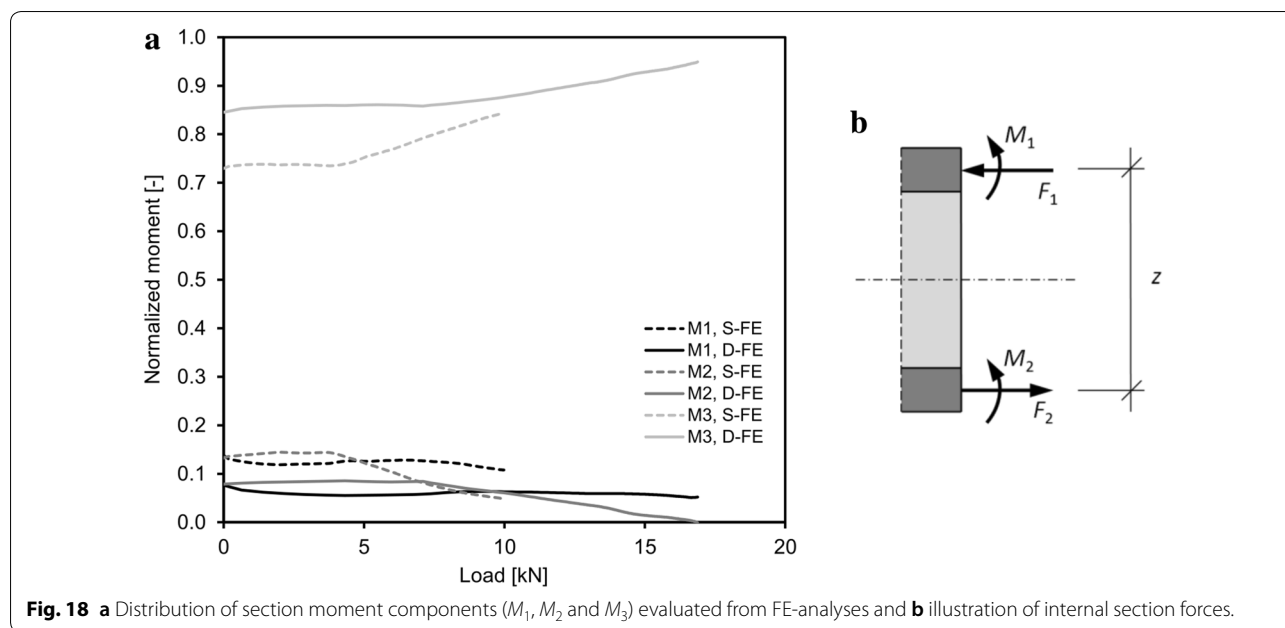
To further compare the connector performance, the development of the shear angles at the ends of the beams, i.e. 50 and 2400 mm, were compared to the experimental results plotted against the normalized load in Fig. 14 (Sect. 4.3). The shear angle development from the FEA results is observed to correlate with the experimental results until reaching the maximum load level (ratio of 1.0). After reaching the peak load, as expected, the model is unable to explicitly capture the pull-out failure mechanism. Although the FE model is fairly conservative regarding the stiffness at higher load levels and also neglects connector pull-out failure, it is able to describe the global behaviour up until the maximum element capacity governed by the connector failure and is thought to be a useful tool for determining the ultimate resistance of the sandwich element. The presented results show that the FE modelling approach is appropriate to describe the composite action behaviour of the TRRPC-FC element realistically.

### 5.2.2 Section Moments and Crack Formation

To analyse the resulting composite action, the internal section forces in the sandwich element when subjected to bending are computed according to the schematic in Fig. 18b. Based on equilibrium conditions, it is implied that  $F_1 = F_2$  and the total internal moment  $M$  is the sum of three components as shown in Eq. 8:

$$M = M_1 + M_2 + M_3 = M_1 + M_2 + F_1 z \quad (8)$$

where  $M_1$  and  $M_2$  are the moments resisted by the two RPC panels and  $M_3$  is resisted by the forces  $F_1$  and  $F_2$ , which arise due to composite action between the panels. The distribution between the moments  $M_1$ ,  $M_2$  and  $M_3$  (normalized with respect to the total moment  $M$ ) in the mid-span section of the analysed beams with single connectors (S-FE) and double connectors (D-FE) is described in Fig. 18a.



From Fig. 18a, the moment component ( $M_3$ ) resisted by the composite action is significantly larger than the other two components in both connector configuration cases while being slightly more dominant for the double connectors. Initially, the composite action represents approximately 73% (S-FE) and 86% (D-FE) which corresponds rather well with the experimentally-based values of 69% (S-X) and 87% (D-X) presented in Table 2 (Sect. 4). In both cases, the distribution of the three components is relatively constant until major cracks occur in the lower panel, at a load level of approximately 4 kN for the single connectors (S-FE) and 7 kN for the double connectors (D-FE). Gradually, as the panels undergo further cracking due to increased loading, their moment resistance ( $M_1, M_2$ ) decreases, and as a result,  $M_3$  becomes an increasing percent of the total moment. The crack formation at displacement values of 5 and 10 mm for both configurations can be seen in Fig. 19.

Through further analysis of the crack formation, it can be concluded that the upper panel mainly cracks due to local bending under the loading equipment, while the lower panel cracks over a larger region due to global bending of the element giving rise to tensile forces in the panel. It can be noted that the individual cracks are not captured in the given FE model due to the underlying element definitions, i.e. embedded reinforcement and size of the shell elements being equal to the actual crack distance (40–50 mm). As a result, it is the extent of the cracked regions which is described in the model.

## 6 Conclusions

The mechanical properties of the individual materials, namely RPC, carbon textile grid and GFRP connectors, were experimentally characterized in this study. Four-point bending testing were conducted on large-scale TRRPC-FC elements according to a quasi-static loading scheme to gain an understanding of the associated flexural capacity, level of composite action, deformations, crack propagation and failure mechanisms. The structural behaviour of the developed TRRPC-FC sandwich elements was found to be highly dependent on the stiffness and strength of the GFRP connectors to ensure composite action between the two TRRPC panels. The failure of the sandwich elements was mainly attributed to the connector capacity, which was also greatly influenced by the initiation and progression of connector pull-out from the panels.

The optical measurements based on DIC proved to be an advantageous tool to measure displacements along the length of the TRRPC panels during testing which was subsequently applied to quantify the relative longitudinal displacement between the panels. DIC measurements were also found useful to validate the FE modelling approach.

Both the single and double connector configurations were found to provide sufficient load resistance when compared to the projected loading. The difference can mainly be associated to the stiffness, such that the specimens with double connectors exhibit smaller deflections due to a higher degree of composite action. This observed effect can, to some extent, be compensated for

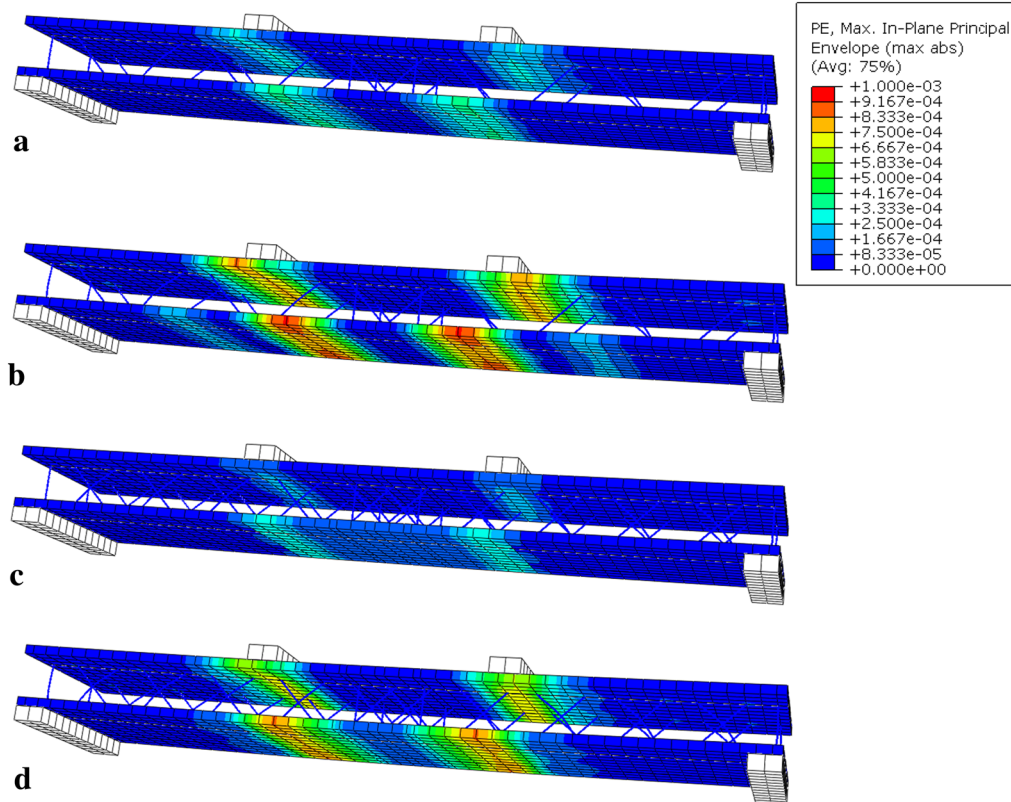


**Fig. 19** Crack formation, represented as plastic strain, in the FE model for the single connector configuration (S FE) at a displacement of **a** 5 mm, **b** 10 mm and for the double connector configuration (D FE) at a displacement of **c** 5 mm and **d** 10 mm. Blue represents no cracking and red represents a fully open crack with no stress transfer.

by using closer spacing between the single connectors in the façade element. Single or double connector configurations can also be used in the elements at different locations of a building depending on the actual design wind load. Another advantage with the double connector configuration is that it can efficiently withstand both wind suction and wind pressure on a façade element.

The developed FE model was found to conservatively describe the stiffness of the sandwich elements at higher load levels as a result of neglecting connector pull-out failure. Moreover, due to the prescribed element type and size, the extent of the cracked regions was solely described in the model. Despite these underlying assumptions, the model was able to describe the global behaviour up until the maximum element capacity governed by the connector failure and is thought to be a useful tool for determining the ultimate resistance of the TRRPC-FC elements.

#### Authors' contributions

MF, UM and NWP designed and produced the sandwich elements; MF designed and performed the various mechanical tests; NWP, MF and DV analyzed the experimental and analytical results and drafted the manuscript. All authors read and approved the final manuscript.

#### Author details

<sup>1</sup> RISE Research Institutes of Sweden, Borås, Sweden. <sup>2</sup> RISE Research Institutes of Sweden, CBI Swedish Cement and Concrete Research Institute, Borås, Sweden.

#### Acknowledgements

The presented research was made possible with the support of the European Community's Seventh Framework Programme under Grant Agreement No. 608950 (SESBE). Further SESBE research project information can be found here: <http://www.sesbe.eu>.

#### Competing interests

The authors declare that they have no competing interests.

#### Publisher's Note

Springer Nature remains neutral with regard to jurisdictional claims in published maps and institutional affiliations.

Received: 6 December 2017 Accepted: 24 July 2018  
Published online: 20 November 2018

#### References

- Colombo, I. G., Colombo, M., & di Prisco, M. (2015). Bending behaviour of textile reinforced concrete sandwich beams. *Construction and Building Materials*, 95, 675–685.
- Dassault Systèmes Abaqus/CAE User's Guide. ABAQUS Version 6.14. 2014.

- EN 206-1. (2013). *Concrete—specification, performance, production and conformity*. Brussels: European Standard.
- Engberts, E. (2006). Large-size facade elements of textile reinforced concrete. In *ICTRC'2006-1st international RILEM conference on textile reinforced concrete* (pp. 309–18). RILEM Publications SARL.
- fib. fib Bulletin No. 74—Planning and design handbook on precast building structures. 1998.
- fib. fib Bulletin No. 40—FRP reinforcement in RC structures. 2007.
- Flansbjerg, M., Honfi, D., Vennetti, D., Mueller, U., Williams Portal, N., & Wlasak, L. (2016). Structural performance of GFRP connectors in composite sandwich façade elements. *Journal of Facade Design and Engineering*, 4, 35–52.
- Ghoneim, G., El-Hacha, R., Carson, G., Zakariasen, D. (2010). Precast ultra high performance fibre reinforced concrete replaces stone and granite on building façade. In *Third international fib congress incorporating the PCI annual convention and bridge conference 2010* (pp. 1–15). Washington, DC: Precast Prestressed Concrete Institute (PCI).
- GOM. (2015). *GOM correlate manual basic, GOM optical measuring techniques*. Braunschweig: GOM.
- Hegger, J., Horstmann, M., & Scholzen, A. (2008). Sandwich panels with thin-walled textile-reinforced concrete facings. *Special Publication*, 251, 109–124.
- Hegger, J., Kulas, C., & Horstmann, M. (2012). Spatial textile reinforcement structures for ventilated and sandwich façade elements. *Advances in Structural Engineering*, 15, 665–675.
- ISO 10406-1. (2008). *Fibre-reinforced polymer*. Geneva: International Organization for Standardization.
- Miccoli, L., Fontana, P., Silva, N., Klinge, A., Cederqvist, C., Kreft, O., et al. (2015). Composite UHPC-AAC/CLC facade elements with modified interior plaster for new buildings and refurbishment. Materials and production technology. *Journal of Facade Design and Engineering*, 3, 91–102.
- Mueller, U., Williams Portal, N., Chozas, V., Flansbjerg, M., Larazza, I., da Silva, N., et al. (2016). Reactive powder concrete for facade elements—a sustainable approach. *Journal of Facade Design and Engineering*, 4, 53–66.
- Mueller, U., Williams Portal, N., Flansbjerg, M., Malaga, K. (2017). Textile reinforced reactive powder concrete and its application for facades. In *Eleventh high performance concrete (11th HPC) and the second concrete innovation conference (2nd CIC)*. Tromsø, 6–8 March 2017.
- Rebentrost, M., Wight, G., Fehling, E. (2008). Experience and applications of ultra-high performance concrete in Asia. In *2nd international symposium on ultra high performance concrete*. (pp. 19–30).
- Shams, A., Stark, A., Hoogen, F., Hegger, J., & Schneider, H. (2015). Innovative sandwich structures made of high performance concrete and foamed polyurethane. *Composite Structures*, 121, 271–279.
- Silva, N., Mueller, U., Malaga, K., Hallingberg, P., Cederqvist, C. (2015). Foam concrete-aerogel composite for thermal insulation in lightweight sandwich facade elements. In *27th biennial national conference of the concrete institute of Australia in conjunction with the 69th RILEM Week*. Melbourne, Australia: Concrete Institute of Australia.
- Stenberg, E. (2013). *Structural systems of the million program era*. Stockholm: KTH School of Architecture.
- Williams Portal, N., Flansbjerg, M., Johannesson, P., Malaga, K., & Lundgren, K. (2015). Tensile behaviour of textile reinforcement under accelerated ageing conditions. *Journal of Building Engineering*, 5, 57–66.

**Submit your manuscript to a SpringerOpen<sup>®</sup> journal and benefit from:**

- Convenient online submission
- Rigorous peer review
- Open access: articles freely available online
- High visibility within the field
- Retaining the copyright to your article

---

Submit your next manuscript at ► [springeropen.com](http://springeropen.com)

---